An NAD$^+$-dependent transcriptional program governs self-renewal and radiation resistance in glioblastoma

Amit D. Gujar[a], Son Le[b], Diane D. Mao[a], David Y. A. Dadey[c,d], Alice Turski[a], Yo Sasaki[e], Diane Aum[a], Jingqin Luo[f,g], Sonika Dahiya[h], Liya Yuan[a], Keith M. Rich[a,g], Jeffrey Milbrandt[e,i], Dennis E. Hallahan[c,g,i,j], Hiroko Yano[a,e,g,i,k], David D. Tran[b], and Albert H. Kim[a,g,i,k,l,1]

[a]Department of Neurological Surgery, Washington University School of Medicine, St. Louis, MO 63110; [b]Lillian S. Wells Department of Neurosurgery, McKnight Brain Institute, University of Florida College of Medicine, Gainesville, FL 32605; [c]Department of Radiation Oncology, Washington University School of Medicine, St. Louis, MO 63110; [d]Medical Scientist Training Program, Washington University School of Medicine, St. Louis, MO 63110; [e]Department of Genetics, Washington University School of Medicine, St. Louis, MO 63110; [f]Division of Biostatistics, Department of Medicine, Washington University School of Medicine, St. Louis, MO 63110; [g]Siteman Cancer Center, Washington University School of Medicine, St. Louis, MO 63110; [h]Department of Pathology and Immunology, Washington University School of Medicine, St. Louis, MO 63110; [i]Hope Center for Neurological Disorders, Washington University School of Medicine, St. Louis, MO 63110; [j]Mallinckrodt Institute of Radiology, Washington University School of Medicine, St. Louis, MO 63110; [k]Department of Neurology, Washington University School of Medicine, St. Louis, MO 63110; and [l]Department of Developmental Biology, Washington University School of Medicine, St. Louis, MO 63110

Edited by Kevin Struhl, Harvard Medical School, Boston, MA, and approved November 14, 2016 (received for review July 12, 2016)

Accumulating evidence suggests cancer cells exhibit a dependency on metabolic pathways regulated by nicotinamide adenine dinucleotide (NAD$^+$). Nevertheless, how the regulation of this metabolic cofactor interfaces with signal transduction networks remains poorly understood in glioblastoma. Here, we report nicotinamide phosphoribosyltransferase (NAMPT), the rate-limiting step in NAD$^+$ synthesis, is highly expressed in glioblastoma tumors and patient-derived glioblastoma stem-like cells (GSCs). High NAMPT expression in tumors correlates with decreased patient survival. Pharmacological and genetic inhibition of NAMPT decreased NAD$^+$ levels and GSC self-renewal capacity, and NAMPT knockdown inhibited the in vivo tumorigenicity of GSCs. Regulatory network analysis of RNA sequencing data using GSCs treated with NAMPT inhibitor identified transcription factor E2F2 as the center of a transcriptional hub in the NAD$^+$-dependent network. Accordingly, we demonstrate E2F2 is required for GSC self-renewal. Downstream, E2F2 drives the transcription of members of the inhibitor of differentiation (ID) helix–loop–helix gene family. Finally, we find NAMPT mediates GSC radiation resistance. The identification of a NAMPT-E2F2-ID axis establishes a link between NAD$^+$ metabolism and a self-renewal transcriptional program in glioblastoma, with therapeutic implications for this formidable cancer.

glioblastoma | NAMPT | NAD$^+$ | self-renewal | radiation resistance

The prognosis for glioblastoma, the most common malignant intrinsic brain tumor in adults, remains poor despite aggressive multidisciplinary therapy, including maximal safe surgical resection, radiation therapy, and temozolomide (1, 2). The failure of these interventions to generate a durable response stems in part from inadequate understanding of the metabolic and molecular mechanisms underlying malignant behavior and therapeutic resistance (3, 4). Nicotinamide adenine dinucleotide (NAD$^+$) has a well-known role in cellular metabolism and is an important cofactor for signaling pathways that regulate aging, inflammation, diabetes mellitus, axonal injury, and cancer (5, 6). Nicotinamide phosphoribosyltransferase (NAMPT), the rate-limiting enzyme in mammalian NAD$^+$ synthesis, produces NAD$^+$ precursor nicotinamide mononucleotide (NMN) to drive NAD$^+$-dependent processes. Interestingly, NAMPT expression is extremely low in the mammalian brain compared with other organs (7, 8). However, NAMPT is highly expressed in several cancers, and features of cancer cells, including proliferation, invasion, and tumor growth, exhibit a dependence on NAD$^+$ (9–11). In noncancer cells, NAD$^+$ plays a critical role in transcriptional control, providing a metabolic basis for epigenetic reprogramming (12–16). Enzymes using NAD$^+$ as a cofactor, including the sirtuins and poly-ADP ribosyl transferases, regulate transcription factor activity and chromatin structure (13–15). Additionally, NAD$^+$ can control transcription by altering DNA methylation in neurons (12). However, in glioblastoma, little is known about NAD$^+$-dependent transcriptional events and whether these events impact malignant behavior and therapy response.

Here, we examine the role of NAD$^+$ regulation and NAD$^+$-dependent transcription in glioblastoma. We demonstrate NAMPT is highly expressed in glioblastoma tumors compared with normal brain tissue. NAMPT inhibition disrupts the self-renewal and in vivo tumorigenicity of human glioblastoma stem-like cells (GSCs), a therapy-resistant cancer subpopulation. Importantly, we identify key regulators of GSC self-renewal in the NAD$^+$-dependent transcriptional program and further examine their role in radiation resistance.

Results

We first asked if the major regulator of the cellular NAD$^+$ pool, NAMPT, has clinical relevance in glioblastoma by interrogating expression data in The Cancer Genome Atlas (TCGA). We found NAMPT mRNA is up-regulated in glioblastoma tumors generally and in tumors of all four molecular subtypes compared

Significance

Glioblastoma, the most common primary malignant brain tumor in adults, remains challenging despite multimodality therapy, necessitating the discovery of new therapies. Nicotinamide adenine dinucleotide (NAD$^+$) plays a pivotal role in cancer cell metabolism, but how NAD$^+$ impacts functional signaling events in glioblastoma is not well understood. We provide clinical evidence that high expression of NAMPT, the rate-limiting step in NAD$^+$ biosynthesis, in glioblastoma tumors is associated with poor overall survival in patients, and demonstrate NAMPT and NAD$^+$ are required for the maintenance of patient-derived glioblastoma stem-like cells (GSCs). Moreover, we delineate a NAD$^+$-dependent transcriptional program that governs GSC self-renewal and dictates the radiation resistance of these cells. These findings identify potential new therapeutic avenues for the treatment of glioblastoma.

Author contributions: A.D.G. and A.H.K. designed research; A.D.G., D.D.M., D.Y.A.D., A.T., Y.S., D.A., and L.Y. performed research; A.D.G., S.L., D.Y.A.D., A.T., J.L., S.D., and A.H.K. analyzed data; K.M.R., J.M., D.E.H., H.Y., and D.D.T. contributed new reagents/analytic tools; K.M.R., J.M., D.E.H., H.Y., and D.D.T. provided conceptual input and critically read the manuscript; A.H.K. provided clinical material and conceived the research project; and A.D.G. and A.H.K. wrote the paper.

The authors declare no conflict of interest.

This article is a PNAS Direct Submission.

[1]To whom correspondence should be addressed. Email: kima@wudosis.wustl.edu.

This article contains supporting information online at www.pnas.org/lookup/suppl/doi:10.1073/pnas.1610921114/-/DCSupplemental.

with normal brain (Fig. 1 *A* and *B*). We then divided TCGA glioblastoma patients into high and low NAMPT mRNA groups and found that patients with high NAMPT-expressing tumors exhibited a shorter overall survival (Fig. 1*C*). An independent dataset, REMBRANDT, revealed a similar inverse correlation between tumor NAMPT expression and patient survival (Fig. 1*D*). NAMPT protein was observed in tumor cells by immunohistochemistry in both *IDH1* WT and mutant glioblastoma tumor sections (Fig. 1*E* and Fig. S1*A*). We found NAMPT expression was also increased in grade 2 and 3 gliomas compared with normal brain (REMBRANDT; Fig. S1*B*) and that *IDH1* mutant and WT tumors of matched grade and histopathology did not significantly differ in NAMPT expression with the exception of grade 3 astrocytomas, which exhibited higher NAMPT expression in *IDH1* WT tumors (TCGA; Fig. S1*C*). Collectively, these data suggest a potential cell-intrinsic role for NAMPT in glioblastoma and potentially more broadly in gliomas.

We have described a human model system for the functional analysis of glioblastoma cells using patient-derived specimens (17). These primary glioblastoma cells, also referred to as GSCs, exhibit the ability to self-renew in vitro and form invasive brain tumors in immunocompromised mice in vivo, providing a robust human model system (17). As in bulk tumors, we observed high NAMPT expression in four GSC lines compared with human astrocytes by quantitative real-time PCR (qPCR) (Fig. 2*A* and Fig. S2 *A*–*C*). Using a specific pharmacological inhibitor of NAMPT, FK866, we examined the biological role of NAMPT in GSC self-renewal, a defining characteristic of GSCs, which often parallels tumor-initiating potential (18). Treatment of GSC lines B18 and B36 with FK866 in vitro decreased NAD^+ levels in a dose-dependent fashion (Fig. 2*B*). Using the extreme-limiting dilution assay (ELDA), we found exposure to NAMPT inhibitor decreased GSC self-renewal capacity in a manner reversible by addition of NMN, the product of NAMPT (Fig. 2*C* and Fig. S2*D*). An alternative approach

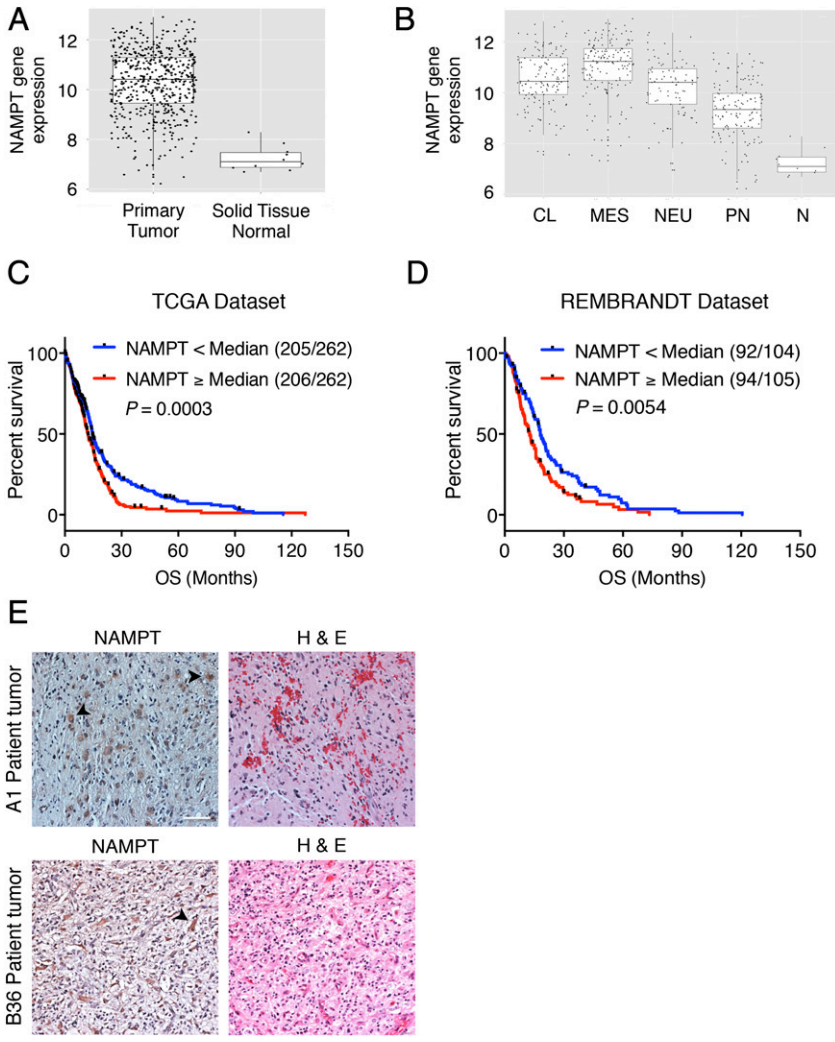

Fig. 1. NAMPT is highly expressed in glioblastoma tumors and its expression has prognostic value in glioblastoma patients. (*A*) Box plot for NAMPT mRNA expression in glioblastoma ($n = 529$) and normal brain tissue samples ($n = 10$) from TCGA (unpaired *t* test, $P = 1.40 \times 10^{-9}$). (*B*) Box plots for NAMPT mRNA expression demonstrate high NAMPT expression in all four molecular subtypes of glioblastoma in TCGA microarray samples compared with normal brain tissue. (*C*) Kaplan–Meier curves show overall survival (OS) from 524 newly diagnosed glioblastoma patients in TCGA based on NAMPT expression. Patients with high NAMPT-expressing tumors (greater than or equal to the median) exhibited decreased OS (log-rank test, $P = 0.0003$). Numbers in parentheses represent number of events/total patients with molecular data. (*D*) Kaplan–Meier curves show OS from 209 glioblastoma patients from the REMBRANDT dataset as in *C*. Patients with high NAMPT-expressing tumors (greater than or equal to the median) exhibited decreased OS (log-rank test, $P = 0.0014$). (*E*) Formalin-fixed, paraffin-embedded 10-μm sections from two glioblastoma patients were subjected to NAMPT immunohistochemistry (*Left*) and hematoxylin and eosin staining (*Right*). Glioblastoma cells (arrowhead) demonstrate NAMPT protein expression. CL, classical; H & E, hematoxylin and eosin staining; MES, mesenchymal; N, normal; NEU, neural; PN, proneural. (Scale bar: 50 μm.)

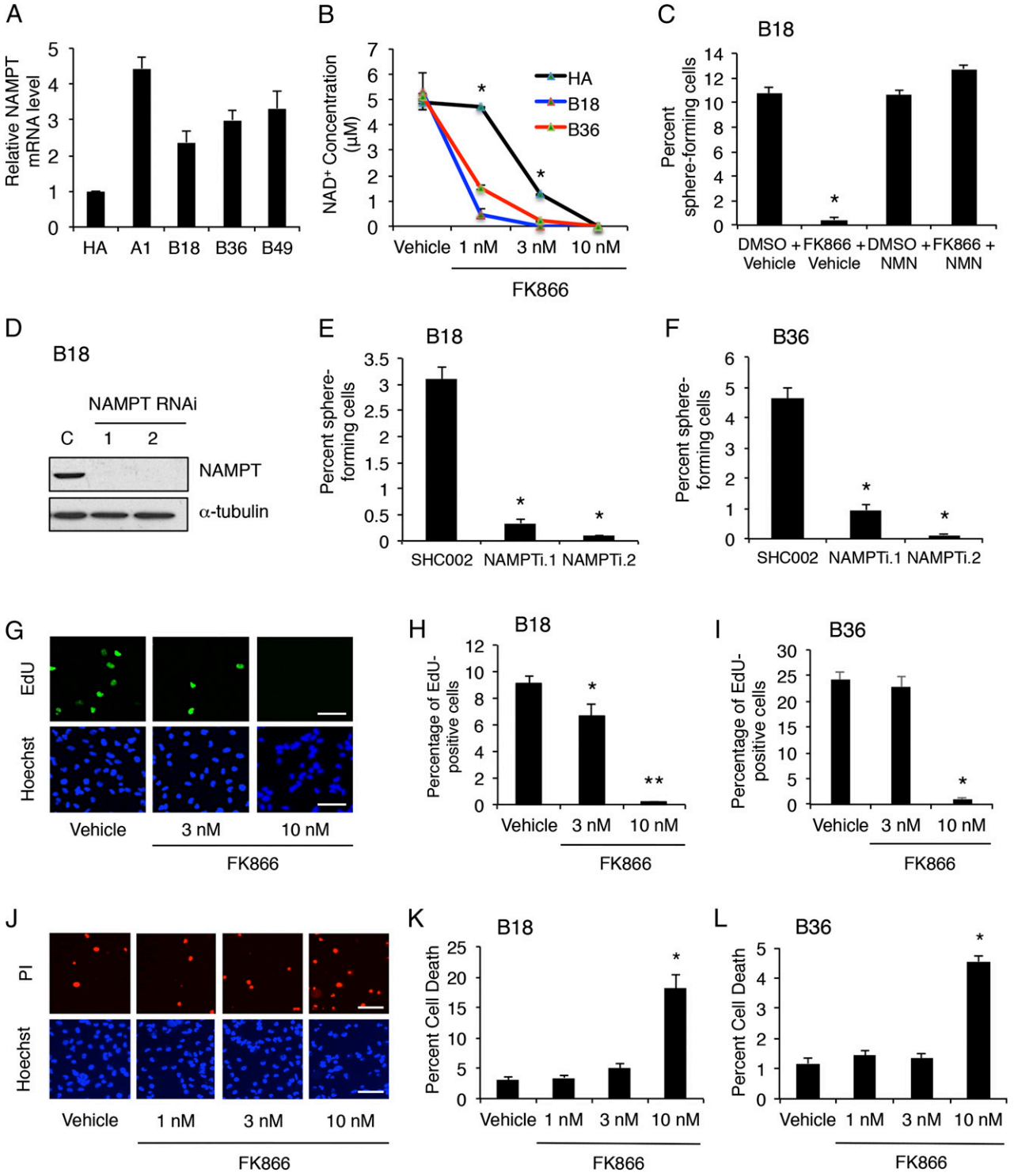

Fig. 2. NAMPT regulates GSC self-renewal capacity. (*A*) RNA was isolated from GSCs or HA, and qPCR performed using *GAPDH* and *ACTB* as reference genes. Data represent mean + SEM. GSC lines express higher levels of NAMPT vs. HA (ANOVA, $P < 0.0001$ for A1, $P < 0.02$ for B18, and $P < 0.005$ for B36 and B49). (*B*) HA and GSC lines treated with FK866 or vehicle for 3 d were subjected to HPLC analysis to determine NAD^+ concentrations. Data represent mean ± SEM. GSCs showed higher sensitivity to FK866 compared with HA (ANOVA, $*P < 0.0001$). (*C*) GSCs treated as indicated were subjected to ELDA. At 14 d later, the number of wells with spheres was analyzed. Data represent mean + SEM. FK866 decreased GSC self-renewal in a manner reversible by NMN (ANOVA, $*P < 0.0001$). (*D*) GSCs transduced with two distinct NAMPT RNAi or control scrambled SHC002 (*C*) lentiviruses were selected with puromycin. At 7 d later, lysates were processed for immunoblotting. (*E* and *F*) GSCs treated as in *D* were subjected to ELDA 3 d after transduction as in *C*. Data represent mean + SEM. NAMPT knockdown decreased the percentage of self-renewing GSCs compared with control SHC002 (ANOVA, $*P < 0.0001$). (*G*) GSCs were treated with FK866 or vehicle for 4 d and then labeled with EdU and Hoechst 33342. (Scale bar: 100 μm.) (*H*) Quantification of EdU-positive cells from *G*. Data represent mean + SEM. FK866 triggered a dose-dependent decrease in cell proliferation (ANOVA, $*P = 0.01$ and $**P < 0.0001$). (*I*) GSCs treated as in *G* were quantified as in *H* (ANOVA, $*P < 0.0001$). (*J*) GSCs were treated with FK866 or vehicle for 4 d and then subjected to the propidium iodide (PI) exclusion assay and Hoechst 33342. (Scale bar: 100 μm.) (*K*) Quantification of PI-positive cells from *J*. Data represent mean + SEM. FK866 triggered cell death in GSCs at 10 nM (ANOVA, $*P < 0.0001$). (*L*) GSCs treated as in *J* were analyzed as in *K* (ANOVA, $*P < 0.0001$).

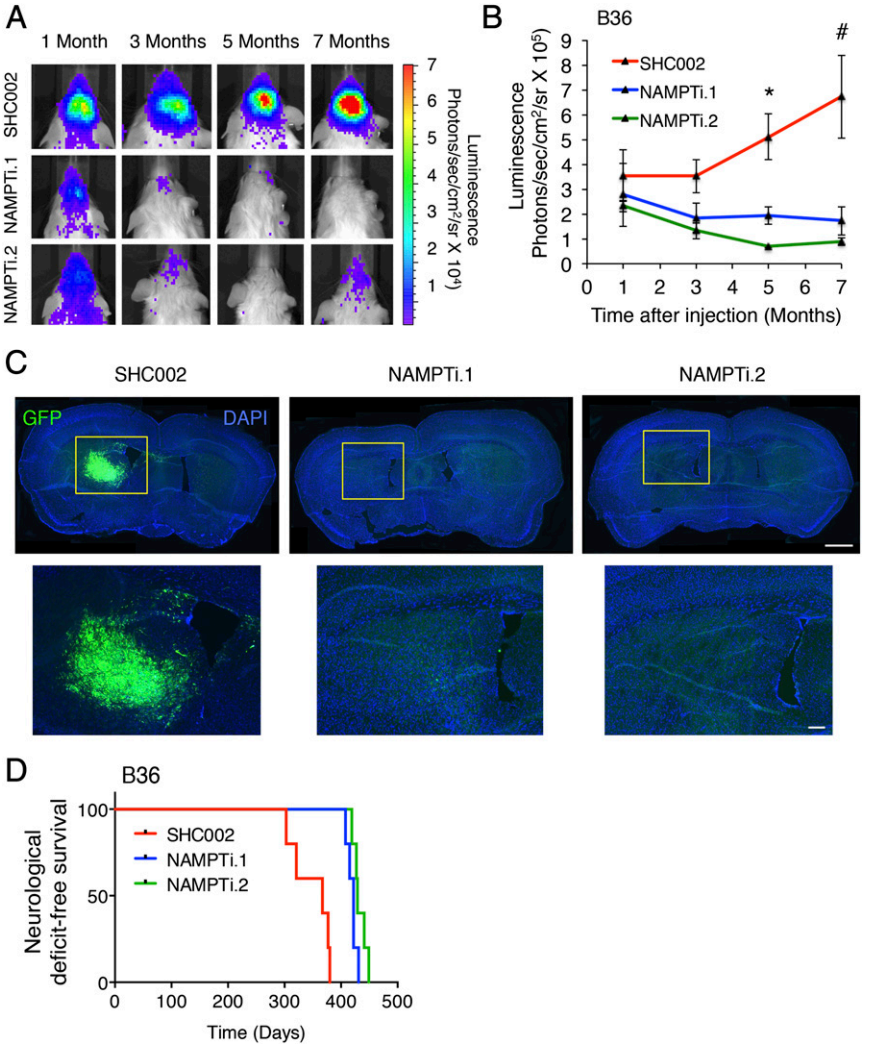

Fig. 3. NAMPT is critical for GSC tumorigenicity in vivo. (*A*) B36 GSCs stably infected with GFP-T2A-luciferase lentivirus were transduced with indicated lentiviruses and injected into the right putamen of NOD-SCIDγ mice. Injected animals were subjected to live BLI. Representative animals at indicated time points after injection are shown ($n = 5$ animals per condition). (*B*) Quantification of BLI signals from animals in *A*. Data represent mean ± SEM. NAMPT knockdown decreased GSC tumorigenicity compared with control SHC002 (ANOVA, $^{*}P = 0.001$ and $^{*}P < 0.0001$ vs. NAMPTi.1 and NAMPTi.2, respectively; $^{\#}P = 0.004$ and $^{\#}P = 0.001$ vs. NAMPTi.1 and NAMPTi.2, respectively; $n = 5$ animals per condition). (*C*) Animals bearing intracranial B36 GSCs as in *A* were killed after 12 mo, and 10-μm-thick brain sections were subjected to GFP immunofluorescence. Nuclei were stained with DAPI. Representative coronal brain sections are shown. (Scale bar: *Upper*, 100 μm; *Lower*, 250 μm.) (*D*) Kaplan–Meier curves demonstrated increased neurological deficit-free survival in animals bearing NAMPT knockdown GSCs compared with those bearing control SHC002-infected GSCs treated as in *A* (log-rank test, $P = 0.0002$; $n = 4$ animals per condition).

using lentiviral shRNAs targeting two distinct regions in the NAMPT gene decreased both NAMPT protein and NAD^+ levels in GSCs (Fig. 2*D* and Fig. S2 *E* and *F*). Importantly, NAMPT RNAi also decreased the frequency of sphere-forming GSCs, indicating NAMPT is essential for GSC self-renewal (Fig. 2 *E* and *F*).

Because the phenomenon of self-renewal represents an integration of a number of distinct cellular events, we asked if NAMPT regulates GSC proliferation or survival (Fig. 2 *G–L*). EdU incorporation experiments demonstrated FK866 inhibits the proliferation of B18 GSCs at 3 nM and of both GSC lines at 10 nM (Fig. 2 *G–I*). The 10 nM FK866 triggered 18% and 4.5% cell death in B18 and B36 GSCs, respectively, with little to no cell death at lower concentrations (Fig. 2 *J–L*). Time-lapse images of B36 GSCs following FK866 treatment showed a plateau in cell number at ∼85 h, followed by an increase in caspase-3/7 activity 10 h later, suggesting proliferation is more sensitive to declining NAD^+ levels compared with survival (Fig. S2 *G* and *H*). Together, these data indicate NAMPT controls GSC self-renewal by regulating both cell proliferation and survival.

To determine if NAMPT is required to propagate tumors in vivo, we generated a B36 GSC line stably expressing GFP-T2A-luciferase, enabling GFP immunofluorescence as well as bioluminescence imaging (BLI) in live animals to assess tumor burden. GSCs infected with two distinct NAMPT RNAi were injected into the brains of NOD-SCIDγ mice, and BLI was performed on these animals over time (Fig. 3*A*). NAMPT knockdown inhibited brain tumor formation by both BLI and GFP immunofluorescence in brain sections (Fig. 3 *A–C*). Importantly, mice bearing NAMPT knockdown GSCs exhibited increased survival compared with mice bearing control-infected GSCs, indicating NAMPT is critical for the in vivo tumorigenicity of GSCs (Fig. 3*D*). To determine if the eventual neurological deficit or death in animals injected with NAMPT RNAi GSCs might be the consequence of failure to completely silence NAMPT expression in tumor cells (as has been reported with other RNAi manipulations) (19), we performed coimmunolabeling for GFP and NAMPT in

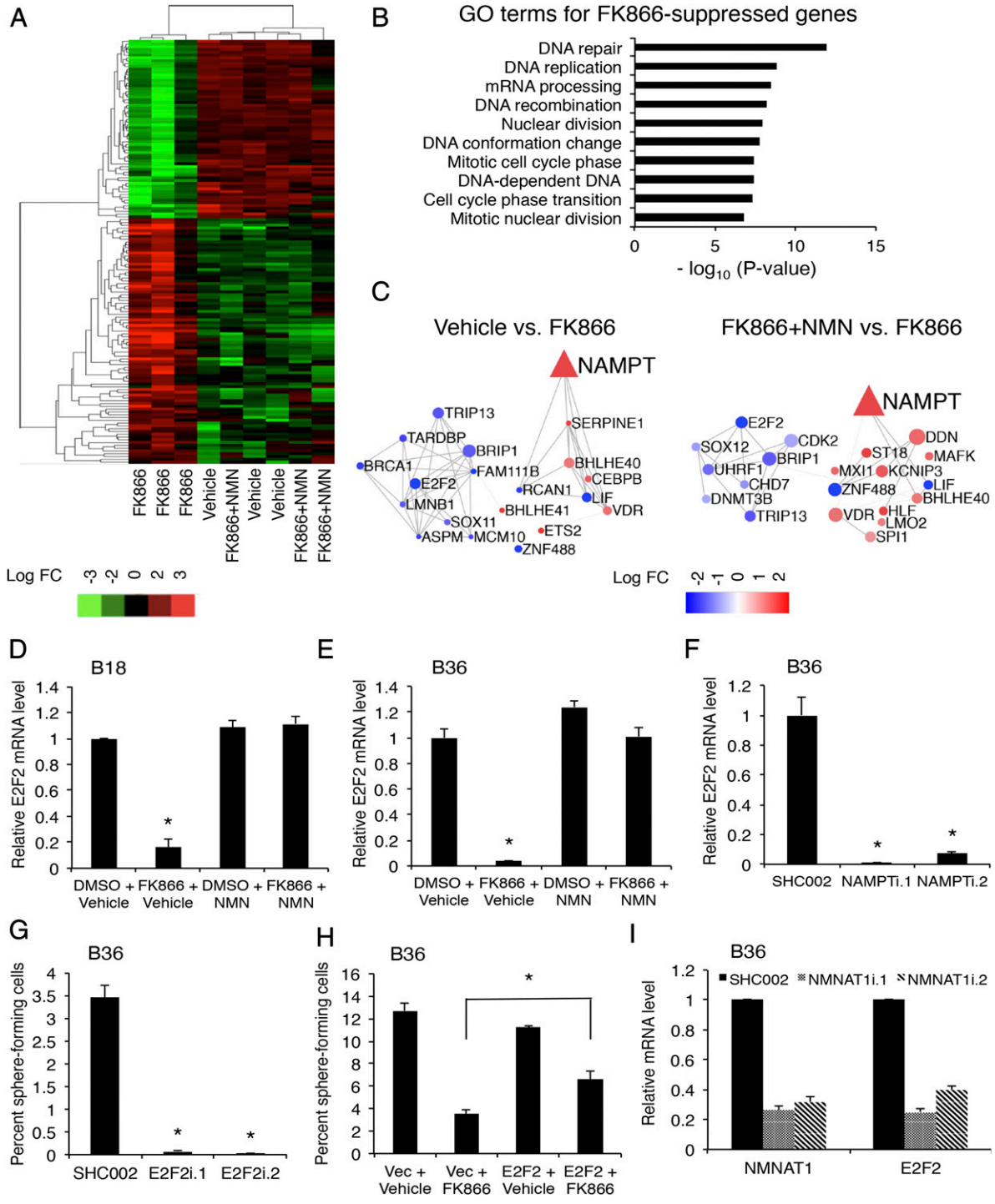

Fig. 4. NAMPT regulates E2F2. (*A*) B18 GSCs were treated with 100 nM FK866 with or without 1 mM NMN for 3 d. RNA was isolated from cells and subjected to RNA-sequencing (RNA-seq). Differentially expressed genes in the RNA-seq dataset with more than eightfold change between maximum and minimum values (total 155 genes) were subjected to hierarchical clustering to generate a heat map. (*B*) Gene Ontology (GO) analysis of the RNA-seq data was performed using R/Bioconductor package GAGE. The top 10 processes enriched in the FK866-suppressed gene set are shown. (*C*) Transcriptional networks were generated from RNA-seq data from TCGA glioblastoma dataset by ARACNe and NAMPT-dependent subnetworks extracted ($n = 169$). The size of a node denotes the number of connections or edges (except for NAMPT). The color of a node denotes the logFC with FK866 (red, up-regulated; blue, down-regulated). (*D* and *E*) GSCs were treated as in *A*; total RNA was extracted and qPCR performed using primers specific to E2F2. Data represent mean + SEM (ANOVA, $^*P < 0.0001$). (*F*) GSCs were transduced with indicated lentiviruses and selected with puromycin. At 7 d after infection, RNA was isolated to determine E2F2 mRNA levels as in *D*. Data represent mean + SEM (ANOVA, $^*P < 0.0001$). (*G*) B36 GSCs transduced with indicated lentiviruses and selected with puromycin for 2 d were subjected to ELDA as in Fig. 2*C*. Data represent mean + SEM. E2F2 knockdown decreased GSC self-renewal (ANOVA, $^*P < 0.0001$). (*H*) GSCs infected with E2F2-overexpressing (or control vector) lentiviruses were subjected to ELDA as in Fig. 2*C* in the presence of FK866 (3 nM) or vehicle. Data represent mean + SEM. FK866 decreased self-renewal compared with vehicle (ANOVA, $P < 0.0001$). Expression of E2F2 plus FK866 increased self-renewal compared with infection with Vec plus FK866 (ANOVA, $^*P = 0.005$). (*I*) RNA was extracted from GSCs transduced with the indicated lentiviruses 5 d postinfection, and qPCR was performed using indicated primers. Data represent mean + SEM. NMNAT1 knockdown decreased E2F2 mRNA levels (ANOVA, $P < 0.0001$).

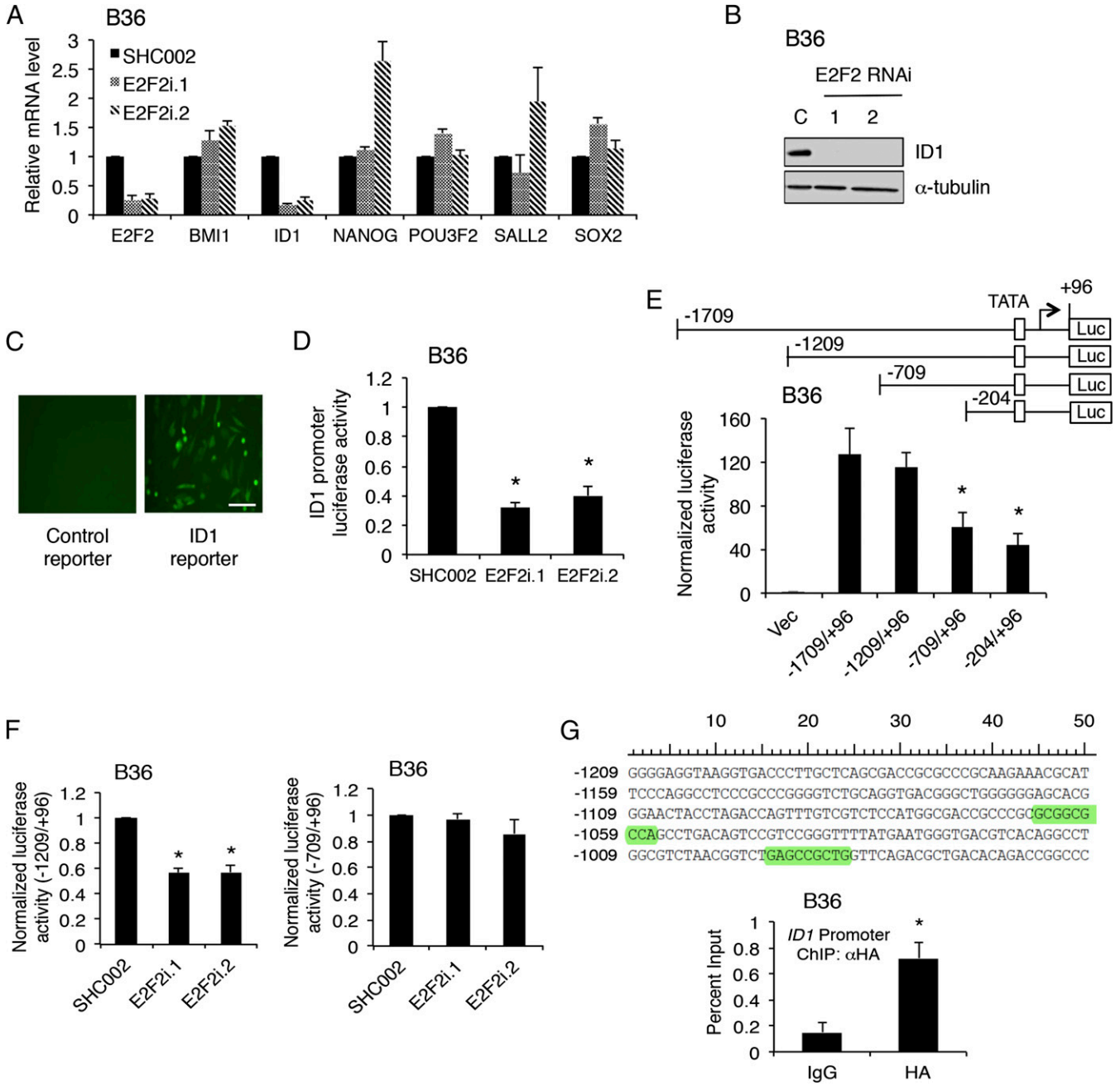

Fig. 5. E2F2 is required for GSC self-renewal and directly regulates ID1. (*A*) RNA was extracted from GSCs transduced with the indicated lentiviruses 7 d after infection, and qPCR was performed using indicated primers. Data represent mean + SEM. E2F2 knockdown reduced ID1 mRNA levels (ANOVA, $P < 0.0001$). (*B*) GSCs treated as in *A* were processed for immunoblotting. (*C*) B36 GSCs were stably infected with *ID1* promoter-driven GFP-T2A-luciferase reporter or promoterless control (pGreenfire1). (Scale bar: 50 μm.) (*D*) GSCs stably expressing ID1 reporter as in *D* were transduced with indicated lentiviruses and subjected to luciferase assay after 7 d. Luciferase values were normalized by total protein (control SHC002 = 1). Data represent mean + SEM. E2F2 knockdown decreased ID1 reporter activity (ANOVA, $^*P < 0.005$). (*E*, *Upper*) Schematic depicting *ID1* promoter deletions. (*E*, *Lower*) Indicated *ID1* promoter-Firefly luciferase plasmids (pGL2 basic) were transfected into GSCs along with Renilla-expressing plasmid. At 36 h later, cells were assayed for luciferase activity. Luciferase values were divided by Renilla values and normalized to the activity of the control vector (=1). Data represent mean + SEM. *ID1* promoter activity was significantly diminished in the −709/+96 and −204/+96 reporters compared with the −1709/+96 reporter (ANOVA, $^*P < 0.01$). (*F*) GSCs stably infected with either −1209/+96 (*Left*) or −709/+96 (*Right*) *ID1* promoter reporter lentiviruses were transduced with the indicated lentiviruses and subjected to luciferase assay as in *E* after 7 d. Data represent mean + SEM. E2F2 knockdown decreased −1209/+96 but not −709/+96 ID1 reporter activity (ANOVA, $^*P < 0.0001$). (*G*, *Upper*) Evolutionarily conserved E2F2 motifs among seven mammals between −1209 and −1009 from the TSS of the *ID1* gene are highlighted. (*G*, *Lower*) GSCs were transduced with lentiviruses expressing HA-tagged E2F2 and processed for ChIP using anti-HA or isotype control antibody. Primers specific for the genomic region from −1209 to −1009 from the *ID1* TSS were then used for qPCR, and values plotted as percent input. Data represent mean + SEM. HA-E2F2 ChIP-qPCR significantly enriched for the *ID1* promoter compared with control ChIP-qPCR (unpaired *t* test, $^*P = 0.007$; $n = 4$).

NAMPT RNAi and control tumors. Indeed, we observed occasional NAMPT$^+$ cells in tumor cells arising from NAMPT RNAi-infected GSCs at 12 mo (Fig. S3).

We next wanted to understand the mechanism of how NAMPT governs GSC maintenance. Because NAD$^+$ is known to control transcription in other cellular contexts, we examined the global

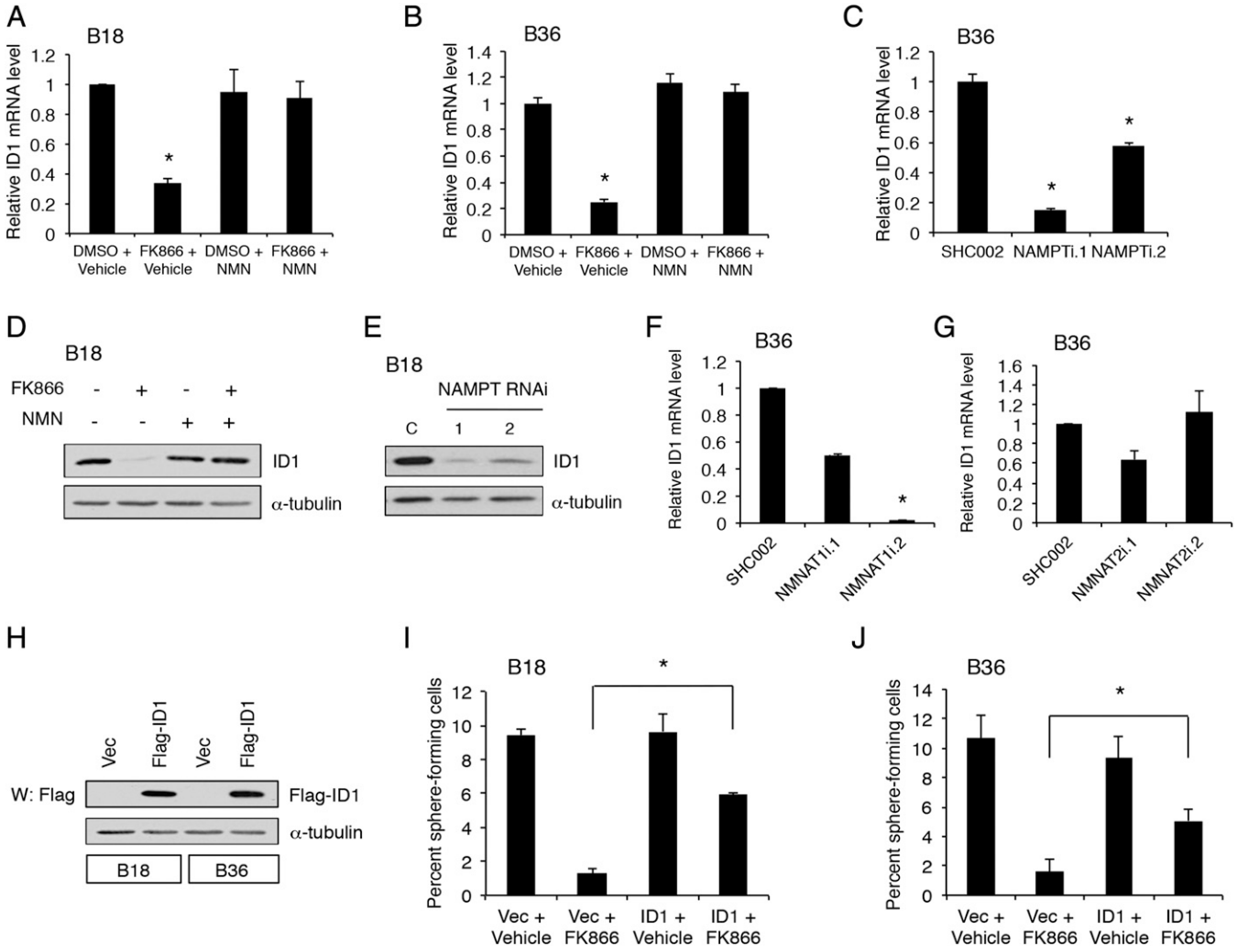

Fig. 6. NAMPT regulates ID1 expression to drive GSC self-renewal. (*A*) GSCs were treated with 100 nM FK866 or vehicle with or without 1 mM NMN for 3 d. RNA was extracted, and qPCR was performed using primers specific to ID1. Data represent mean + SEM (ANOVA, $*P < 0.005$). (*B*) GSCs were treated and subjected to qPCR as in *A*. Data represent mean + SEM (ANOVA, $*P = 0.001$). (*C*) GSCs transduced with indicated lentiviruses were selected with puromycin. At 7 d later, qPCR performed as in *A*. Data represent mean + SEM (ANOVA, $*P < 0.0001$). (*D*) Lysates from GSCs treated as in *A* were processed for immunoblotting. (*E*) Lysates from GSCs treated as in *C* were processed for immunoblotting. (*F* and *G*) RNA was extracted from GSCs transduced with the indicated lentiviruses 5 d postinfection, and qPCR was performed using indicated primers. Data represent mean + SEM. NMNAT1 knockdown reduced ID1 mRNA levels (ANOVA, $*P < 0.005$). (*H*) GSCs were stably transduced with FLAG-tagged ID1-expressing or control vector (Vec) lentiviruses. Lysates from GSCs were processed for immunoblotting. (*I*) GSCs stably infected as in *H* were subjected to ELDA as in Fig. 2*C* in the presence of FK866 or vehicle. FK866 = 10 nM. Data represent mean + SEM. FK866 decreased self-renewal compared with vehicle (ANOVA, $P < 0.0001$). Expression of ID1 plus FK866 increased self-renewal compared with infection with Vec plus FK866 (ANOVA, $*P < 0.0001$). (*J*) GSCs treated as in *I* were subjected to ELDA as in Fig. 2*C*. FK866 = 3 nM. Data represent mean + SEM. FK866 decreased self-renewal compared with vehicle (ANOVA, $P < 0.0001$). Expression of ID1 plus FK866 increased self-renewal compared with infection with Vec plus FK866 (ANOVA, $*P = 0.015$).

transcriptional consequences of NAD^+ depletion in GSCs. GSCs were exposed to FK866 with or without NMN and subjected to RNA-sequencing (RNA-seq). NAMPT inhibition altered the levels of 581 protein-coding genes, with 307 down-regulated genes (52.8%; Fig. 4*A* and Dataset S1). No significant changes in the transcriptome were observed between vehicle- and FK866 plus NMN-treated GSCs (Fig. 4*A*). Gene ontogeny analysis of genes down-regulated by NAMPT inhibitor demonstrated enrichment in processes related to DNA repair and replication, nuclear division, and cell cycle phase transition, consistent with the role of NAMPT in GSC self-renewal and tumor growth (Fig. 4*B*). To identify critical nodes within the NAD^+-driven transcriptional network, we used two parallel bioinformatics approaches. We used regulatory network analysis—Algorithm for the Reconstruction of Accurate Cellular Networks (ARACNe)—with the 169 RNA-seq glioblastoma datasets in TCGA to first build a transcriptional network and then generated NAMPT-regulated subnetworks by extracting network connections containing significantly altered transcripts in FK866-treated glioblastoma cells (Fig. 4*C* and Tables S1 and S2) (20). Genes predicted to be master regulators would be hypothesized to exhibit a change in transcript levels and also have a high number of connections with other genes in the network (Tables S1 and S2). Among these genes, transcription factor *E2F2* was notable as having the highest number of connections in the FK866 treatment subnetwork, suggesting an important transcriptional hub. In parallel, with the same NAMPT-dependent RNA-seq data, we used iRegulon to detect transcription factors and their targets, with the goal of identifying transcription factors with a high number of targets within the same dataset and therefore more likely to represent an upstream regulator of the NAMPT-dependent transcriptional program (21). A DNA motif-based algorithm again identified E2F2 as the most significant, differentially expressed transcription factor

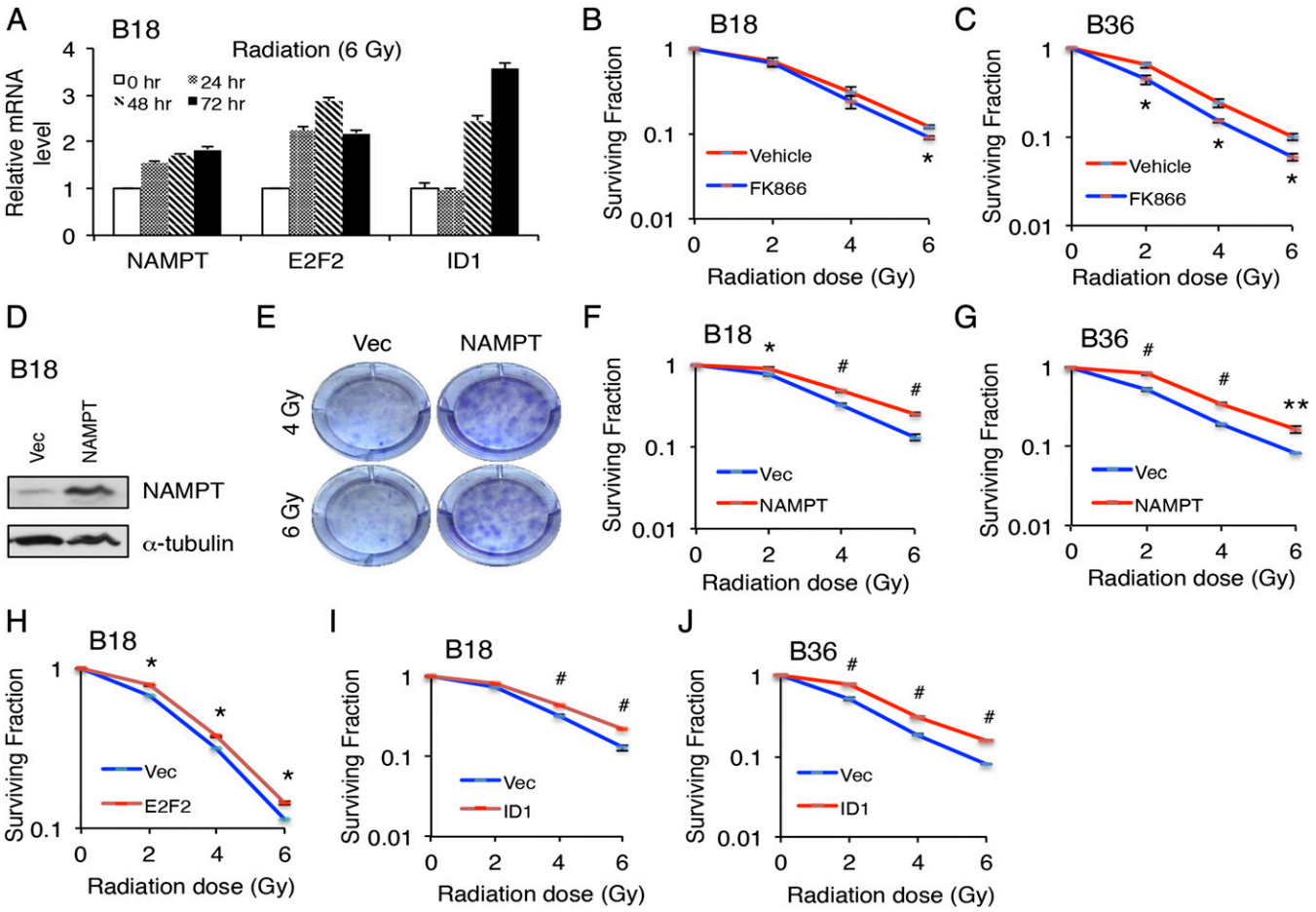

Fig. 7. NAMPT promotes GSC radioresistance. (*A*) GSCs were treated with 6 Gy IR and harvested at indicated time points. RNA was extracted, and qPCR was performed using indicated primers. Data represent mean + SEM. IR treatment increased NAMPT, E2F2, and ID1 mRNA levels (ANOVA, $P < 0.005$ for NAMPT and $P < 0.0001$ for E2F2 at all post-IR time points, $P \leq 0.005$ at 48 and 72 h for ID1). (*B*) GSCs were treated with 1 nM FK866 or vehicle for 2 d and plated at clonogenic density in medium containing FK866 or vehicle. IR treatment was performed the following day, and clonogenic survival was determined 14 d after IR by staining colonies with 0.5% cresyl violet. The number of colonies was counted to determine the surviving fraction. Data represent mean ± SEM (unpaired *t* test, $^{*}P < 0.05$). (*C*) GSCs were treated with 3 nM FK866 or vehicle for 2 d and plated at clonogenic density in medium containing FK866 or vehicle. Clonogenic survival was determined after IR as in *B*. Data represent mean ± SEM (unpaired *t* test, $^{*}P < 0.05$). (*D*) GSCs were transduced with NAMPT-expressing or control vector (Vec) lentiviruses and selected with puromycin. At 4 d later, lysates were processed for immunoblotting. (*E*) GSCs treated with indicated lentiviruses were plated at clonogenic density after selection with puromycin. IR was performed the following day, and colonies were stained with 0.5% cresyl violet 14 d after IR. Representative images of wells are shown. (*F* and *G*) GSCs were transduced with indicated lentiviruses, and clonogenic survival after IR was determined as in *B*. Data represent mean ± SEM (unpaired *t* test, $^{*}P < 0.05$, $^{\#}P < 0.005$, $^{**}P < 0.01$). (*H*) GSCs were transduced with indicated lentiviruses, and clonogenic survival after IR was determined as in *B*. Data represent mean ± SEM (unpaired *t* test, $^{*}P < 0.05$). (*I* and *J*) GSCs were transduced with indicated lentiviruses, and clonogenic survival after IR was determined as in *B*. Data represent mean ± SEM (unpaired *t* test, $^{\#}P < 0.005$).

with 383 putative targets in the NAMPT-dependent RNA dataset. We therefore focused on E2F2 as a potential critical upstream transcription factor controlling the NAD^+-dependent transcriptional network. We verified in GSCs that both FK866 and NAMPT knockdown dramatically decrease E2F2 levels in a manner reversible by NMN (Fig. 4 *D*–*F* and Fig. S4*A*).

To test the functional significance of E2F2 in glioblastoma, we transduced GSCs with two lentiviral shRNAs targeting E2F2 and subjected them to the extreme-limiting dilution assay. E2F2 knockdown reduced GSC self-renewal capacity and proliferation, consistent with the effects of NAMPT inhibition (Fig. 4*G* and Fig. S4*B*). To determine if E2F2 lies functionally downstream of NAMPT, we performed epistasis experiments combining NAMPT inhibitor with E2F2 overexpression (Fig. 4*H*). FK866 inhibited the self-renewal capacity of GSCs, which was partially but significantly rescued by E2F2 overexpression, suggesting E2F2 acts downstream of NAMPT. Consistent with this linear order, NMN could not rescue the self-renewal deficit triggered by E2F2 RNAi (Fig. S4*C*). To determine the mechanism by which NAMPT regulates E2F2 expression, we examined the nicotinamide mononucleotide adenylyltransferases (NMNATs), a family of catalytic enzymes that convert NMN to NAD^+ with a particular focus on NMNAT1, which is localized to the nucleus and is responsible for generating the nuclear NAD^+ pool (22). Knockdown of NMNAT1, but not of the related Golgi-resident family member NMNAT2, effectively decreased E2F2 mRNA levels, indicating NMNAT1 links NAMPT to E2F2 expression (Fig. 4*I* and Fig. S4*D*).

To determine the downstream mechanism of E2F2 in GSCs, we performed a candidate-based miniscreen for possible E2F2 targets by examining a set of genes known to be associated with self-renewal following E2F2 RNAi in GSCs (Fig. 5*A*) (18, 23–25). Among these genes, E2F2 RNAi consistently decreased the levels of helix–loop–helix gene inhibitor of differentiation 1 (ID1) (Fig. 5*A*). E2F2 knockdown also decreased ID1 protein levels in GSCs (Fig. 5*B*). Because the ID proteins represent a family of four members, we asked if E2F2 more generally controlled expression of the ID gene family. E2F2 RNAi decreased mRNA levels of ID1, ID2, and ID3, but not ID4, suggesting E2F2 may transcriptionally activate *ID1–3*

(Fig. S5 *A*–*C*). To test if *ID* genes are direct targets of E2F2, we focused on *ID1* as a representative family member and generated an *ID1* promoter reporter encoding GFP-T2A-luciferase driven by a previously reported 2-kb sequence upstream of the *ID1* transcription start site (TSS) (26). Transduction of the ID1 reporter in GSCs generated a robust GFP and luciferase signal compared with control (Fig. 5*C*). E2F2 RNAi diminished ID1 reporter activity, indicating endogenous E2F2 regulates the *ID1* promoter (Fig. 5*D*). Deletion analysis revealed a substantial decrease in *ID1* promoter activity when removing the sequence spanning −1209 to −709 from the TSS (Fig. 5*E*). E2F2 RNAi decreased the activity of the −1209/+96 ID1 reporter but had no effect on the −709/+96 reporter, suggesting an E2F2-binding site exists between −1209 and −709 (Fig. 5*F*). Examination of the genomic sequence in this region revealed two evolutionarily conserved E2F2 motifs (Fig. 5*G*). Indeed, similar E2F2 binding sites were found in evolutionarily conserved regions of the promoters for both *ID2* and *ID3* but not *ID4* (Fig. S5 *D* and *E*). To test if E2F2 directly binds the ID1 promoter at this locus, we performed ChIP using GSCs stably expressing HA epitope-tagged E2F2. Anti-HA ChIP followed by qPCR using primers specific to the *ID1* promoter region harboring the predicted E2F2 sites demonstrated E2F2 directly binds to the *ID1* promoter in GSCs (Fig. 5*G*). Together, these results indicate E2F2 directly controls ID1 transcription in human GSCs.

We next tested if NAMPT also regulates ID1 expression in GSCs. Both pharmacological and genetic inhibition of NAMPT decreased ID1 mRNA and protein levels (Fig. 6 *A*–*E*). Moreover, consistent with the E2F2 results, knockdown of NMNAT1, but not NMNAT2, decreased ID1 mRNA levels (Fig. 6 *F* and *G*), together suggesting a NAMPT-NMNAT1-E2F2 pathway to ID1. To test if ID1 biologically acts downstream of NAMPT, we performed epistasis experiments in assays of GSC self-renewal (Fig. 6 *H*–*J*). FK866 substantially inhibited the self-renewal capacity of GSCs, which was partially but significantly restored by ID1 overexpression, suggesting ID1 operates downstream of NAMPT (Fig. 6 *H*–*J*). Together, these results indicate the NAMPT–E2F2–ID axis represents an important transcriptional signaling pathway that governs GSC self-renewal.

We next asked if this NAD^+-driven transcriptional program might be clinically relevant in the response to radiation therapy in GSCs. Initial qRT-PCR experiments using B18 GSCs revealed that NAMPT, E2F2, and ID1 mRNA levels increase after treatment with ionizing radiation (IR), with ID1 levels increasing in a slightly delayed fashion, consistent with its role as an E2F2 target (Fig. 7*A*). These gene expression changes could potentially represent a cellular defense to IR, a pathway contributing to IR toxicity, or an epiphenomenon. We therefore treated GSCs with sublethal concentrations of FK866, subjected them to different doses of IR, and assessed clonogenic survival 2 wk later. Interestingly, NAMPT inhibition increased GSC responsiveness to IR (Fig. 7 *B* and *C*), and in complementary experiments, NAMPT overexpression decreased GSC responsiveness to radiation, together indicating that NAMPT promotes radiation resistance (Fig. 7 *D*–*G*). Quantification of γH2AX foci in GSCs following IR suggested that the initial burden of DNA double-strand breaks is not significantly different in cells treated with FK866 or overexpressing NAMPT, suggesting instead that downstream responses to IR are altered by NAMPT manipulation (Fig. 4*B* and Fig. S6). Finally, we tested if the transcriptional consequences of NAMPT might also be important for GSC radiation responsiveness. Initial experiments to test the direct role of E2F2 in radiation responsiveness using E2F2 RNAi revealed that E2F2 is necessary for GSC survival at clonogenic density in the absence of IR, precluding additional manipulations using IR in the setting of E2F2 knockdown (Table S3). However, the complementary experiment of E2F2 overexpression modestly but significantly increased GSC radioresistance (Fig. 7*H*). Accordingly, ID1 overexpression also increased GSC radioresistance (Fig. 7 *I* and *J*). Together, these results implicate the NAMPT-E2F2-ID1 pathway in the biological response of GSCs to radiation therapy.

Discussion

We have examined the NAD^+-dependent transcriptional program in GSCs and defined a NAMPT-E2F2-ID signaling pathway, which regulates GSC self-renewal and radiation resistance. NAMPT is expressed at high levels in several different cancers and, therefore, this enzyme has been considered a potential therapeutic cancer target (5, 9, 27). Recent studies in glioblastoma have indicated specific genetic subgroups may be exquisitely sensitive to NAMPT inhibition (28, 29). *IDH1* mutation sensitizes GSCs to NAMPT inhibitors due to low ambient levels of NAD^+, resulting from down-regulation of nicotinic acid phosphoribosyltransferase (NAPRT1), which catalyzes an alternative NAD^+ salvage pathway (29). MYC overexpression and *MYC* or *N-MYC* amplification in glioblastoma cells increase glycolytic flux and lower NAD^+ levels, similarly leading to increased susceptibility to NAMPT inhibitors (28). The relevance of the NAMPT–E2F2–ID pathway to these specific molecular contexts is an interesting question for future investigation. It should be noted, however, that inhibiting NAMPT carries therapeutic challenges, because systemic NAMPT inhibition is known to cause retinal toxicity and potential blindness (30). Therefore, local NAMPT inhibitory strategies or disruption of the tumor-specific signals regulating NAMPT or its downstream consequences need to be carefully considered for potential clinical translation.

Before this study, the precise role of E2F2 in glioblastoma has remained enigmatic because deregulated E2F2 levels in both directions have been shown to inhibit glioblastoma cell functions. For instance, overexpression of E2F2 in U343 cells induced apoptosis (31), whereas E2F2 knockdown inhibited the tumorigenicity of U87MG cells (32). We found that NAMPT and NMNAT1 are required for E2F2 expression, which is essential for self-renewal in human GSCs. It is likely that tightly regulated levels of E2F2 are needed for appropriate control of S-phase entry, self-renewal, and cell survival. An important mechanistic question is how nuclear NAD^+ levels regulate E2F2 mRNA in GSCs. In addition to its metabolic functions, NAD^+ can influence transcriptional programs as a cofactor for NAD^+-dependent enzymes, including the sirtuins, poly- and mono-ADP ribosyl transferases, and ADP ribosyl cyclases. Which specific nuclear NAD^+-dependent events lead to E2F2-ID remains to be determined.

The biological roles and mechanisms of ID family proteins in glioblastoma have been the subject of intense recent investigation (23, 33–36). Benezra and colleagues (23) identified a self-renewing subpopulation expressing high levels of Id1 in a PDGFB-driven $Arf^{-/-}$ mouse model of glioblastoma. More recently, combined genetic deletion of *Id1*, *Id2*, and *Id3* in a *HrasV12* and p53 knockdown-driven mouse model of high-grade glioma inhibited in vivo tumorigenicity and caused GSC exit from the perivascular niche, suggesting functional redundancy among Id family members (35). However, acute knockdown of ID1 alone in human GSCs was sufficient to reduce tumor formation in vivo, suggesting compensatory mechanisms for acute ID1 loss may be less robust (36).

We found the NAMPT-E2F2-ID1 pathway is up-regulated in GSCs following radiation and represents a protective response to radiation. Consistent with our results, E2F2 was found to have a protective role in radiation-induced, p53-independent apoptosis in *Drosophila* third-instar larvae (37). ID1 has recently been shown to be necessary for prostaglandin E2-mediated radiation resistance in mouse glioblastoma cells, and $ID1^+$ human GSCs appear to be relatively radiation resistant (33). It is likely that additional NAD^+-dependent consequences independent of E2F2 and ID1 also play a role in GSC radioresistance.

Methods

Cell Culture. The generation of patient-derived GSC lines has been described (17). Informed consent was obtained from patients for use of human tissue and cells. All protocols using human tissue were approved by the Institutional Review Board (Washington University). Briefly, patient tumor specimens were mechanically and enzymatically dissociated (Accutase; Sigma-Aldrich). The cell

suspension was passed through a 70-μm cell strainer and plated in RHB-A medium (Clontech) with EGF and FGF-2 (20 ng/mL; PeproTech) on Primaria plates coated with poly-L-ornithine and laminin (Sigma-Aldrich). Cells were strictly used between passage numbers 5–20 for experiments. Human astrocytes (Lonza or generous gift from Milan Chheda, Washington University, St. Louis) were cultured in astrocyte growth media (ScienCell), and HEK293 cells were cultured in DMEM media with 10% (vol/vol) FBS. All cells were incubated at 37 °C with 5% (vol/vol) CO_2. For lentiviral transduction, virus was added with 4 μg/mL polybrene to cells for 4 h. For self-renewal, clonogenic survival, and in vivo tumorigenicity experiments, puromycin was added the day after infection, and cells were used after 48–72 h.

Extreme Limiting Dilution Analysis. Cells were plated at fivefold serial dilutions, from 3,000 to 1 cell/well in ultra-low attachment 96-well plates (Corning Costar). The number of wells containing spheres was counted 14 d later to determine percent sphere-forming cells by ELDA software (38).

Orthotopic Xenotransplantation. Animals were used in accordance with a protocol approved by the Animal Studies Committee at Washington University and compliant with the recommendations of the Guide for the Care and Use of Laboratory Animals (NIH). A total of 250,000 cells were injected into the right putamen of 6- to 9-wk-old NOD-SCIDγ mice using a stereotactic apparatus at the following coordinates: 0.98 mm rostral to bregma, 1.5 mm lateral, and 2.6 mm deep (Hope Center Animal Surgery Core).

Ionizing Radiation Treatment and Clonogenic Survival Analysis. Cells seeded at defined cell densities according to radiation dose were plated and allowed to attach overnight. The next day, cells were irradiated with 0, 2, 4, or 6 Gy. Two weeks later, colonies were stained with 0.5% cresyl violet, and the number of colonies was counted manually in a blinded fashion. Counts represent surviving fraction relative to control.

ACKNOWLEDGMENTS. We thank members of the A.H.K. and H.Y. laboratories, as well as Dr. Gavin Dunn, for helpful discussion. This work was supported by NIH Grant K08NS081105; an American Cancer Society-Institutional research grant; the Concern Foundation; and the Duesenberg Research Fund (A.H.K.). The Genome Technology Access Center is partially supported by National Cancer Institute Cancer Center Support Grant P30 CA91842 and by Institute of Clinical and Translational Sciences/Clinical and Translational Science Awards Grant UL1TR000448 from the National Center for Research Resources, a component of the NIH, and NIH Roadmap for Medical Research. The Molecular Imaging Center at Washington University was funded by National Cancer Institute/NIH P50/CA09056.

1. Sathornsumetee S, et al. (2007) Molecularly targeted therapy for malignant glioma. *Cancer* 110(1):13–24.
2. Stupp R, et al.; European Organisation for Research and Treatment of Cancer Brain Tumor and Radiotherapy Groups; National Cancer Institute of Canada Clinical Trials Group (2005) Radiotherapy plus concomitant and adjuvant temozolomide for glioblastoma. *N Engl J Med* 352(10):987–996.
3. Bao S, et al. (2006) Glioma stem cells promote radioresistance by preferential activation of the DNA damage response. *Nature* 444(7120):756–760.
4. Chen J, et al. (2012) A restricted cell population propagates glioblastoma growth after chemotherapy. *Nature* 488(7412):522–526.
5. Garten A, et al. (2015) Physiological and pathophysiological roles of NAMPT and NAD metabolism. *Nat Rev Endocrinol* 11(9):535–546.
6. Araki T, Sasaki Y, Milbrandt J (2004) Increased nuclear NAD biosynthesis and SIRT1 activation prevent axonal degeneration. *Science* 305(5686):1010–1013.
7. Revollo JR, et al. (2007) Nampt/PBEF/Visfatin regulates insulin secretion in beta cells as a systemic NAD biosynthetic enzyme. *Cell Metab* 6(5):363–375.
8. Kitani T, Okuno S, Fujisawa H (2003) Growth phase-dependent changes in the subcellular localization of pre-B-cell colony-enhancing factor. *FEBS Lett* 544(1-3):74–78.
9. Galli U, et al. (2013) Medicinal chemistry of nicotinamide phosphoribosyltransferase (NAMPT) inhibitors. *J Med Chem* 56(16):6279–6296.
10. van Horssen R, et al. (2013) Intracellular NAD(H) levels control motility and invasion of glioma cells. *Cell Mol Life Sci* 70(12):2175–2190.
11. Wang B, et al. (2011) NAMPT overexpression in prostate cancer and its contribution to tumor cell survival and stress response. *Oncogene* 30(8):907–921.
12. Chang J, et al. (2010) Nicotinamide adenine dinucleotide (NAD)-regulated DNA methylation alters CCCTC-binding factor (CTCF)/cohesin binding and transcription at the BDNF locus. *Proc Natl Acad Sci USA* 107(50):21836–21841.
13. Ghosh S, George S, Roy U, Ramachandran D, Kolthur-Seetharam U (2010) NAD: A master regulator of transcription. *Biochim Biophys Acta* 1799(10-12):681–693.
14. Imai S, Armstrong CM, Kaeberlein M, Guarente L (2000) Transcriptional silencing and longevity protein Sir2 is an NAD-dependent histone deacetylase. *Nature* 403(6771):795–800.
15. Kim MY, Mauro S, Gévry N, Lis JT, Kraus WL (2004) NAD+-dependent modulation of chromatin structure and transcription by nucleosome binding properties of PARP-1. *Cell* 119(6):803–814.
16. Lin SJ, Guarente L (2003) Nicotinamide adenine dinucleotide, a metabolic regulator of transcription, longevity and disease. *Curr Opin Cell Biol* 15(2):241–246.
17. Mao DD, et al. (2015) A CDC20-APC/SOX2 signaling axis regulates human glioblastoma stem-like cells. *Cell Reports* 11(11):1809–1821.
18. Suvà ML, et al. (2014) Reconstructing and reprogramming the tumor-propagating potential of glioblastoma stem-like cells. *Cell* 157(3):580–594.
19. Chudnovsky Y, et al. (2014) ZFHX4 interacts with the NuRD core member CHD4 and regulates the glioblastoma tumor-initiating cell state. *Cell Reports* 6(2):313–324.
20. Margolin AA, et al. (2006) Reverse engineering cellular networks. *Nat Protoc* 1(2):662–671.
21. Janky R, et al. (2014) iRegulon: From a gene list to a gene regulatory network using large motif and track collections. *PLOS Comput Biol* 10(7):e1003731.
22. Berger F, Lau C, Dahlmann M, Ziegler M (2005) Subcellular compartmentation and differential catalytic properties of the three human nicotinamide mononucleotide adenylyltransferase isoforms. *J Biol Chem* 280(43):36334–36341.
23. Barrett LE, et al. (2012) Self-renewal does not predict tumor growth potential in mouse models of high-grade glioma. *Cancer Cell* 21(1):11–24.
24. Molofsky AV, et al. (2003) Bmi-1 dependence distinguishes neural stem cell self-renewal from progenitor proliferation. *Nature* 425(6961):962–967.
25. Romero-Lanman EE, Pavlovic S, Amlani B, Chin Y, Benezra R (2012) Id1 maintains embryonic stem cell self-renewal by up-regulation of Nanog and repression of Brachyury expression. *Stem Cells Dev* 21(3):384–393.
26. Nehlin JO, Hara E, Kuo WL, Collins C, Campisi J (1997) Genomic organization, sequence, and chromosomal localization of the human helix-loop-helix Id1 gene. *Biochem Biophys Res Commun* 231(3):628–634.
27. Chiarugi A, Dölle C, Felici R, Ziegler M (2012) The NAD metabolome–a key determinant of cancer cell biology. *Nat Rev Cancer* 12(11):741–752.
28. Tateishi K, et al. (2016) Myc-driven glycolysis is a therapeutic target in glioblastoma. *Clin Cancer Res* 22(17):4452–4465.
29. Tateishi K, et al. (2015) Extreme vulnerability of IDH1 mutant cancers to NAD+ depletion. *Cancer Cell* 28(6):773–784.
30. Zabka TS, et al. (2015) Retinal toxicity, in vivo and in vitro, associated with inhibition of nicotinamide phosphoribosyltransferase. *Toxicol Sci* 144(1):163–172.
31. Dirks PB, Rutka JT, Hubbard SL, Mondal S, Hamel PA (1998) The E2F-family proteins induce distinct cell cycle regulatory factors in p16-arrested, U343 astrocytoma cells. *Oncogene* 17(7):867–876.
32. Nakahata AM, Suzuki DE, Rodini CO, Fiuza ML, Okamoto OK (2014) RNAi-mediated knockdown of E2F2 inhibits tumorigenicity of human glioblastoma cells. *Oncol Lett* 8(4):1487–1491.
33. Cook PJ, et al. (2016) Cox-2-derived PGE2 induces Id1-dependent radiation resistance and self-renewal in experimental glioblastoma. *Neuro-oncol* 18(10):1379–1389.
34. Lasorella A, Benezra R, Iavarone A (2014) The ID proteins: master regulators of cancer stem cells and tumour aggressiveness. *Nat Rev Cancer* 14(2):77–91.
35. Niola F, et al. (2013) Mesenchymal high-grade glioma is maintained by the ID-RAP1 axis. *J Clin Invest* 123(1):405–417.
36. Soroceanu L, et al. (2013) Id-1 is a key transcriptional regulator of glioblastoma aggressiveness and a novel therapeutic target. *Cancer Res* 73(5):1559–1569.
37. Wichmann A, Uyetake L, Su TT (2010) E2F1 and E2F2 have opposite effects on radiation-induced p53-independent apoptosis in Drosophila. *Dev Biol* 346(1):80–89.
38. Hu Y, Smyth GK (2009) ELDA: Extreme limiting dilution analysis for comparing depleted and enriched populations in stem cell and other assays. *J Immunol Methods* 347(1-2):70–78.
39. Verhaak RG, et al.; Cancer Genome Atlas Research Network (2010) Integrated genomic analysis identifies clinically relevant subtypes of glioblastoma characterized by abnormalities in PDGFRA, IDH1, EGFR, and NF1. *Cancer Cell* 17(1):98–110.